zene *vs.* $CDCl_3$) makes some contribution to the entropy differences.

A change in the nature of X^- results in rather marked changes in both the enthalpies and entropies of activation for $[Co(acac)_2(X)(py)]$ isomerization. In fact, a linear relationship is observed between ΔH^* and ΔS^*. Such an isokinetic relationship is indicative of a common mechanism for the three processes.[19,20] The slope of the isokinetic plot is 406 K (133°C). This is the isokinetic temperature, *i.e.* the temperature at which the rates of all three processes become equal. Verification of the validity of this relationship comes from the Arrhenius plots (Figure 3), which do in fact intersect at this isokinetic temperature. Such verification is necessary, since systematic errors in ΔH^* measurements can result in an apparent linear relationship between ΔH^* and ΔS^*.[21] The trend in activation energies can be attributed to the effect of X^- on the stability of the trigonal bipyramid. Similar reasoning may be invoked to rationalize the trends in the activation entropies. With a π acceptor such as nitrite destabilizing the intermediate, it may be that the intermediate is not a true trigonal bipyramid but distorted to something between this and a square-pyramidal intermediate. That the same effect is acting upon both the ΔH^* and ΔS^* would account for the linear relationship which is observed.

It is interesting to note the change in ΔH^* with nonleaving groups for the aquation of *trans*-$[Co(en)_2(X)(Cl)]^+$. The spread between the extreme values, $X^- = NO_2^-$ to $X^- = OH^-$, is ~5 kcal/mol.[18] This is in marked contrast to the spread of ~14 kcal/mol for *trans*-$[Co(acac)_2(X)(py)]$ when going from $X^- = CN^-$ to $X^- = N_3^-$. The increased sensitivity of the activation parameters to the nonleaving anion in the acetylacetonate complexes may be related to weaker σ bonding of the chelate ring. In other words the cobalt atom's ability to respond to change in other ligands is dampened by strong donor chelates like ethylenediamine.

If there were no thermodynamic difference between the trans and cis isomers of $[Co(acac)_2(X)(py)]$, the distribution of the two at equilibrium would be purely statistical and K_{eq} would be 4. This corresponds to a ΔG° of −0.83 kcal/mol, at 29°, which is equal within experimental limits to that observed for $[Co(acac)_2(NCO)(py)]$. In the case of the other two complexes, ΔG° is more positive than the statistical value by a small amount, 0.2–1.0 kcal/mol. In order to discuss the apparent differences in stability of the isomeric forms of the complexes, it is useful to consider the other thermodynamic parameters. The ΔH° values, −3 kcal/mol, are equal for N_3^- and NO_2^-, while the value for NCO^- is more positive by some 8 kcal/mol. The negative ΔH° for $[Co(acac)_2(NO_2)(py)]$ and $[Co(acac)_2(N_3)(py)]$ indicates that the bonding is stronger and the complex more stable for the cis isomer. This would be the case if the complex preferred to have the two strongest σ donors, X^- and py, cis to one another. Trans effect arguments reason that a good σ-donor group would prefer a weaker donor (*i.e.*, an acetylacetonate oxygen) trans to it.[22] The positive ΔH° for $[Co(acac)_2(NCO)(py)]$ may indicate that NCO^- is the weakest of the three X^- ligands in terms of its bonding to the cobalt.

Acknowledgment. The authors wish to acknowledge the support of this research by the National Science Foundation *via* Grant GP-23464 and partial support by the donors of the Petroleum Research Fund, administered by the American Chemical Society. The authors also wish to acknowledge the use of the NMR Facility for Biochemical Research.

Registry No. $Co(acac)_2$, 14024-48-7; py, 110-86-1; *trans*-$[Co(acac)_2(N_3)(py)]$, 37646-79-0; *trans*-$[Co(acac)_2(CN)(py)]$, 40864-82-2; *trans*-$[Co(acac)_2(NO_2)(py)]$, 14220-10-1; *trans*-$[Co(acac)_2(NCO)(py)]$, 40864-84-4.

(19) J. E. Leffler, *J. Org. Chem.*, **20**, 1202 (1955).
(20) G. C. Lalor, *J. Inorg. Nucl. Chem.*, **31**, 1206 (1969).
(21) R. C. Petersen, *J. Org. Chem.*, **29**, 3133 (1964).
(22) J. M. Pratt and R. G. Thorp, *Advan. Inorg. Chem. Radiochem.*, **12**, 375 (1969).

Contribution from the Department of Chemistry, University of Wisconsin, Madison, Wisconsin 53706

A Voltammetric Study of the Coordinative Reactions of Pyridine with Bis(maleonitriledithiolate)cobalt Complexes

IAN G. DANCE

Received March 6, 1973

Stationary electrode voltammetry (voltage scan rates, 0.01–500 V sec^{-1}) is used to determine the dynamic characteristics in acetonitrile solution of the coordination of pyridine to bis(maleonitriledithiolate)cobalt complexes, $[Co(mnt)_2]^z$, in two oxidation states, $z = 1-, 2-$. Peaks due to the reduction of $[Co(mnt)_2py]^-$ and $[Co(mnt)_2py_2]^-$ and the oxidation of $[Co(mnt)_2py]^{2-}$ are identified; $[Co(mnt)_2py_2]^{2-}$ was not detected at room temperature. The rate and equilibrium constants for the formation of the mono- and bispyridine adducts of the oxidized complex are evaluated, and an order of magnitude estimate is obtained for the formation of $[Co(mnt)_2py]^{2-}$. A brief exposition of the pertinent voltammetric theory is appended.

Introduction

Electrochemical studies of the electron-transfer reactions characteristic of transition metal dithiolene complexes[1] have been directed mainly toward establishment of the existence of electron-transfer series of complexes, determination of the number of electrons transferred, assessment of the lifetimes of highly reduced or oxidized species, determination of comparative redox potentials, and analysis for com-

(1) J. A. McCleverty, *Progr. Inorg. Chem.*, **10**, 49 (1968).

plex concentration. It has generally been assumed that the complexes under investigation were not involved in nonredox coordinative equilibria:[2,3] in cases of adducts known (from other experimental techniques) to be partially dissociated in solution, electrochemical studies were avoided.[4-6]

However, electrochemical methods are potentially of considerable value for investigation of the kinetic and equilibrium properties of homogeneous[7] *non-electron-transfer* reactions undergone by the reactants and/or products of the electron-transfer process.[8] Amine adducts of $[Co(mnt)_2]^-$ [9,10] and their formation equilibria in solution have been studied spectrophotometrically.[11,12] This paper reports a cyclic voltammetry study of $[Co(mnt)_2]^-$ and $[Co(mnt)_2]^{2-}$ in acetonitrile solution in the presence of pyridine, which has permitted further characterization of the solution species and the dynamics of their interconversions.

The theory for the effects of elementary homogeneous processes on the observables in a stationary electrode voltammetric experiment has been presented by Nicholson and Shain.[13] Numerical evaluations of the model were also provided, but in terms of *composite* dependent and independent variables, and limited by special cases necessitated by computational approximations. One such variable (χ) combines the experimental voltage scan rate with the rate constants and equilibrium constant for the homogeneous process. In a second composite variable the experimental potential is combined with the homogeneous process equilibrium constant. However, the use of cyclic voltammetry in characterization of coupled homogeneous processes depends initially on qualitative diagnosis of the *direct* experimental observables,[14] E_p (or $E_{p/2}$) and $i_p v^{-1/2}$, according to the independent experimental variables (the scan rate v, the concentrations of reactants in solution, and possibly the temperature[15]) in terms of chemical models. In order to facilitate such qualitative or semiquantitative analysis, the theoretical behavior has been reexpressed in terms of the straightforward experimental variables for a continuous range of models of the homogeneous processes (see Appendix). This interpretational aid becomes more valuable when there are present competitive homogeneous processes involving both reactants and products of the electron-transfer reaction. Quantitative theory for the voltammetry of this latter circumstance, frequently encountered in dithiolene complex chemistry, has not yet been presented.

Experimental Section

Reagents. Tetra-*n*-butylphosphonium (Bu_4P^+) salts $(Bu_4P)_2[Co(mnt)_2]$, $(Bu_4P)_2[Co(mnt)_2]_2$, $(Bu_4P)_2[Ni(mnt)_2]$, and $(Bu_4P)[Ni(mnt)_2]$ were prepared, purified, and characterized as described elsewhere.[16] Bu_4PClO_4 was prepared by precipitation from equimolar aqueous solutions of Bu_4PCl and $NaClO_4$, recrystallized at least three times from ethanol–water, and dried for 48 hr *in vacuo* at 50°. Acetonitrile was distilled from calcium hydride, then from P_4O_{10}, and stored over 3A molecular sieves. Pyridine was distilled and stored over 5A molecular sieves.

Apparatus. The electrochemical cell (volume *ca.* 30 ml) consisted of a working electrode compartment separated from the auxiliary electrode (a coil of platinum wire) by a coarse grade glass frit. The Luggin capillary was connected to the reference compartment by a medium grade glass frit. A saturated KCl calomel electrode was dipped into the reference compartment, with a loose plug of filter paper separating the aqueous and acetonitrile phases. The working electrode was a platinum sphere (*ca.* 1 mm diameter) constructed by fusing a platinum wire sealed into a glass capillary. A similar electrode of approximately half the diameter and a platinum disk electrode (Beckman No. 39273) were used to vary the current density.

The potentiostat and signal generator were constructed according to standard operational amplifier design. Display was on a Hewlett-Packard X-Y recorder or a Tektronix oscilloscope with camera. Positive feedback from the current follower to the control amplifier was not employed as a means of correcting for residual uncompensated cell resistance.

Results and Discussion

All experiments were performed in purified acetonitrile solution, with tetra-*n*-butylphosphonium perchlorate supporting electrolyte, a platinum sphere working electrode, and saturated KCl calomel electrode. The observed cyclic voltammograms may be influenced by factors extraneous to the coordinative processes of interest, such as uncompensated cell resistance,[17] cation–anion associative equilibria,[3] and the monomer–dimer equilibrium for $[Co(mnt)_2]_n^{n-}$. In order to estimate the magnitude of these effects some background experiments were performed. The voltammetry of the $[Ni(mnt)_2]^{1-/2-}$ system under comparable conditions was recorded as an indicator of uncompensated resistance and ion association effects, and the $[Co(mnt)_2]_n^{n-}$ system was investigated in the absence of pyridine to observe the effects of the monomer–dimer equilibrium.

Voltammetry of the $[Ni(mnt)_2]^{1-/2-}$ System. In Figure 1 are contained typical results for the dependence of peak potential and anodic and cathodic peak current functions[14] on the potential scan rate and on the supporting electrolyte concentration. The separation of anodic and cathodic peak potentials, ΔE_p, is seen to be independent of scan rate up to about $v = 3$ V sec^{-1} and then increases. Similarly, the normalized current function decreases by about 30% as the scan rate increases from 0.3 to *ca.* 200 V sec^{-1}. Both effects are only very slightly dependent on supporting electrolyte concentration.

(2) (a) The thermodynamic and mechanistic aspects of monomer–dimer associative equilibria for iron and cobalt complexes were not evaluated in polarographic studies of dimeric complexes in solution; (b) A. L. Balch, I. G. Dance, and R. H. Holm, *J. Amer. Chem. Soc.*, 90, 1139 (1968); (c) A. L. Balch, *Inorg. Chem.*, 10, 388 (1971).

(3) Cation–anion association for $(Et_4N)_2[Ni(mnt)_2]$ in acetonitrile was included in Lingane's analysis: P. J. Lingane, *Inorg. Chem.*, 9, 1162 (1970).

(4) J. A. McCleverty, N. M. Atherton, N. G. Connelly, and C. J. Winscom, *J. Chem. Soc. A*, 2242 (1969).

(5) G. R. Eaton and R. H. Holm, *Inorg. Chem.*, 10, 805 (1971).

(6) J. Miller and A. L. Balch, *Inorg. Chem.*, 10, 1410 (1971).

(7) The term "homogeneous" is used in this paper to specify all processes in solution which do *not* involve the polarized working electrode; electron transfer with the electrode is the "heterogeneous" process.

(8) For an example from metalloporphyrin chemistry, see D. G. Davis and D. J. Orleron, *Anal. Chem.*, 38, 179 (1966).

(9) 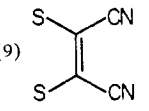 ≡ mnt (maleonitriledithiolate).

(10) This complex ion exists as the dimer $[Co(mnt)_2]_2^{2-}$ in the crystal and in acetonitrile solution,[2b] but all adducts are monomeric. The monomeric formula (abbreviated also to $[CoS_4]^-$) is used here when the state of association is immaterial and the purpose is to differentiate the complex oxidation level from the reduced form $[Co(mnt)_2]^{2-}$ ($[CoS_4]^{2-}$).

(11) C. H. Langford, E. Billig, S. I. Shupack, and H. B. Gray, *J. Amer. Chem. Soc.*, 86, 2958 (1964).

(12) I. G. Dance and T. R. Miller, unpublished results.

(13) R. S. Nicholson and I. Shain, *Anal. Chem.*, 36, 706 (1964).

(14) $E_p \equiv$ voltammetric peak potential; $E_{p/2} \equiv$ potential (on the leading slope) where $i = i_p/2$; $i_p \equiv$ voltammetric peak current; $v \equiv$ scan rate, linear with time. The scan-rate-normalized current function is $iv^{-1/2}$.

(15) R. P. Van Duyne and C. N. Reilley, *Anal. Chem.*, 44, 153 (1972).

(16) I. G. Dance and P. J. Solstad, *J. Amer. Chem. Soc.*, submitted for publication.

(17) The peak potential shifts at high voltage scan rates (high currents) due to residual uncompensated resistance between the working electrode and the Luggin capillary are qualitatively similar to those of the homogeneous[7] processes under investigation: R. S. Nicholson, *Anal. Chem.*, 37, 667 (1965).

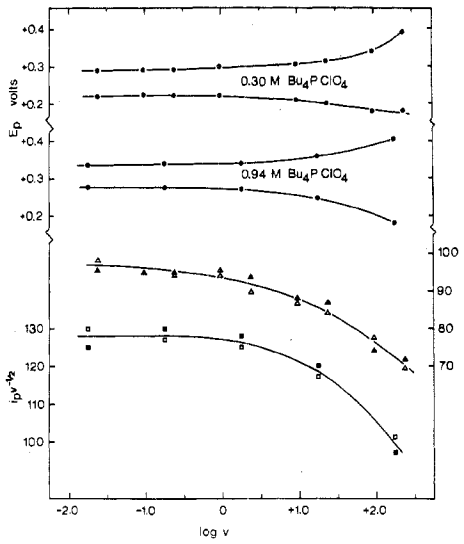

Figure 1. Peak potentials (E_p *vs.* sce) and normalized peak currents ($i_p/v^{1/2}$) as a function of voltage scan rate v (V/sec) for the cyclic voltammogram of the $[Ni(mnt)_2]^{1-,2-}$ couple in acetonitrile solution at a stationary platinum sphere electrode. In the lower section of the figure the cathodic currents are represented with filled symbols and the anodic currents with empty symbols. Supporting electrolyte, $(Bu_4P)ClO_4$, concentrations 0.30 M (triangles, $(Bu_4P)_2[Ni(mnt)_2]$ 1.48×10^{-3} M) and 0.94 M (squares, $(Bu_4P)_2[Ni(mnt)_2]$ 2.89×10^{-3} M).

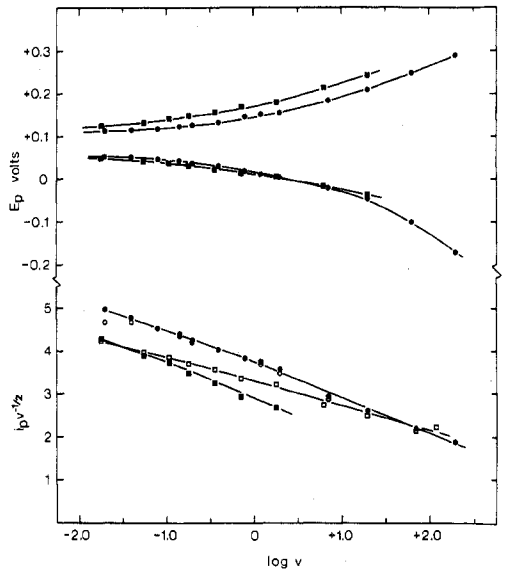

Figure 2. Peak potentials (E_p *vs.* sce) and normalized currents ($i/v^{1/2}$) as a function of voltage scan rate v (V/sec) for the cyclic voltammogram of the $^1/_2[Co(mnt)_2]_2^{2-} \rightleftarrows [Co(mnt)_2]^{2-}$ couple in acetonitrile solution at a stationary platinum electrode. Supporting electrolyte, $(Bu_4P)ClO_4$, 0.98 M; $[Co(mnt)_2]$ formal concentration 2.92×10^{-3} F. Data for a solution of $[Co(mnt)_2]_2^{2-}$ as circles; data for a solution of $[Co(mnt)_2]^{2-}$ as squares. In the lower section of the figure, cathodic currents are represented with filled symbols and anodic currents with empty symbols.

At high scan rates the dependence of the peak potentials and current functions on the current density was checked by threefold variation of the electrode surface area. In the solution containing 0.935 M supporting electrolyte, there was no measurable change in the current function shown in Figure 1, but there was a small E_p shift. The largest potential shift was 20 mV for a current change of 350–1350 μA[18] (at $v = 180$ V sec^{-1}), which permits the conclusion that the observed peak potentials in all other experiments under these conditions are unlikely to be in error by more than about 20 mV.

The current and potential functions in Figure 1, being dependent on the scan rate at high scan rates, reflect low-energy very fast homogeneous processes. It is presumed that association of $[Ni(mnt)_2]^{2-}$ with Bu_4P^+ is one such process.[3,19] It is reasonable to assume that similar effects occur in the $[Co(mnt)_2]^{1-/2-}$ system in acetonitrile, underlying the dimerization and adduct formation equilibria, and therefore the nickel observations are utilized as the background to be subtracted from the observations with cobalt.

$[Co(mnt)_2]^{1-/2-}$ Voltammetry in the Absence of Pyridine. Figure 2 shows current and potential functions for the $[Co(mnt)_2]_2^{2-} \rightleftarrows 2[Co(mnt)_2]^{2-}$ couple in acetonitrile, with 0.98 M supporting electrolyte. Under all conditions one anodic and one cathodic peak is observed, and it is known[2b] that one electron is transferred per cobalt. Compared with the $[Ni(mnt)_2]^{1-/2-}$ system there is, with increasing scan rate, greater increase of the peak potential separation ΔE_p and greater decrease of both oxidation and reduction current functions. This indicates the presence of additional fast chemical processes associated with the electron transfer. However, the continuing changes in the current and potential functions at the highest scan rates mean that the processes are too fast to be "resolved" electrochemically (that is, reaction half times are $\lesssim 10^{-2}$ sec at millimolar concentrations).

The directions of peak potential shift [$\Delta(E_p^c)/\Delta \log v$ negative, $\Delta(E_p^a)/\Delta \log v$ positive] are indicative of chemical steps succeeding the electron transfer in each case, whereas the decreases in normalized current with increasing scan rate reveal the kinetic influence of preceding chemical steps. Thus, there are present equilibria involving both the oxidized and reduced complexes. Reasonable descriptions of the oxidation and reduction pathways are presented in Scheme I.

Scheme I. Oxidation and Reduction Pathways ($[CoS_4] \equiv [Co(mnt)_2]$)

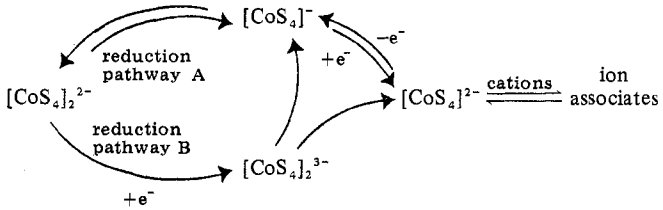

These reactions are generally consistent with the voltammetric observations, but it is not possible to define detailed mechanisms unequivocally.

As before, the behavior of Figure 2 may be regarded as the background for the observations described in the following.

Voltammetry in the Presence of Pyridine. The electrochemistry of the $[Co(mnt)_2]^{1-/2-}$-pyridine system has not been previously recorded. Reported here is the cyclic voltammetry of 2.0×10^{-3} M $(Bu_4P)[Co(mnt)_2]$[10] in acetonitrile with 0.3 M Bu_4PClO_4 supporting electrolyte, as a function of pyridine concentration and voltage scan rate. Scheme II presents all chemical and redox equilibria possible in solution (excluding those of Scheme I) together with the symbolism to be used in discussion of the processes. The coordinative equilibria for mono- and bispyridine adducts

(18) The simplest estimate of the uncompensated cell resistance is therefore 20 ohms.

(19) Preferred association of Bu_4P^+ with $[Ni(mnt)_2]^{2-}$ over $[Ni(mnt)_2]^-$ is also consistent with the positive shift of $E_{1/2}$ with increasing Bu_4PClO_4 concentration but is not proven without data on junction potential variation.

Scheme II. Coordinative and Electron-Transfer Processes ($[CoS_4] \equiv [Co(mnt)_2]$)

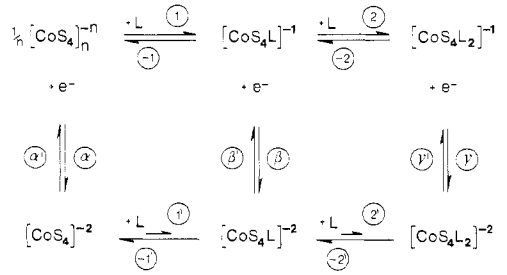

are written horizontally with Arabic numeral identification for both oxidized and reduced $[Co(mnt)_2]$. The connecting redox equilibria with Greek letter symbols are written vertically.

Figures 3–5 contain representative cyclic voltammograms for three solutions containing 10^{-2}, 10^{-1}, and 3 M pyridine, respectively. Spectral analysis[12] of analogous solutions, *without* supporting electrolyte, leads to the following predicted species compositions of the voltammetric solutions: for Figure 3, $[Co(mnt)_2]_2^{2-}$ and $[Co(mnt)_2py]^-$ in ratio *ca.* 1:5; for Figure 4, $[Co(mnt)_2py]^-$ and $[Co(mnt)_2py_2]^-$ in approximately equal concentrations; for Figure 5, only the (cis-octahedral) bis adduct $[Co(mnt)_2py_2]^-$. Figure 6 contains more detailed data for 3 M and neat (12.4 M) pyridine solutions of $(Bu_4P)[Co(mnt)_2py_2]$. Qualitative identification of the voltammetric current peaks with the electron-transfer processes of Scheme II is straightforward. Altogether, three[20] reductive peaks are apparent: a first and second (in terms of increasingly negative potentials) in Figure 3, the second only in Figure 4, and the second and third in Figure 5. The first reduction in Figure 3, clearly apparent at the slowest scan rate, occurs at essentially the same potential as $[Co(mnt)_2]_2^{2-}$ reduction in the absence of pyridine and is process α. The second and third reductions are then β and γ, respectively. Their appearances in the three different solutions are fully consistent with this assignment, as are the relative current changes with scan rate in Figures 3 and 5.

In Figures 3 and 4 only one[20] oxidation peak appears, without substantial dependence of normalized current on scan rate. This current represents the reoxidation associated with the first reduction and therefore is process α'. This assignment is confirmed by the overall similarity to the α' oxidation peak in the absence of pyridine. In Figure 5 only one oxidative current maximum is observed, but at the slowest scan rates (see also Figure 6) it can be seen that there are actually two closely overlapping peaks. The presence of two peaks, rather than one shifting peak, is confirmed by the traces for neat pyridine at seven different scan rates, shown also in Figure 6. The oxidation peak at more negative potential is that of $[Co(mnt)_2py]^{2-}$, electron transfer β' in Scheme II. The argument in support of this assignment is developed below. No evidence of oxidation γ' has been found. The relative values of the reduction potentials for the three electron-transfer equilibria are $E_{\alpha/\alpha'} > E_{\beta/\beta'} > E_{\gamma/\gamma'}$.

The scan rate dependence of the voltammetric traces permits semiquantitative characterization of the coordinative

(20) The section of one trace marked with a broken line in each of the figures represents an extraneous electrode adsorption effect which is observed only at the slowest scan rates. The peak shows characteristic adsorption shape and is not entirely reproducible. It is ignored in the interpretation of the voltammograms.

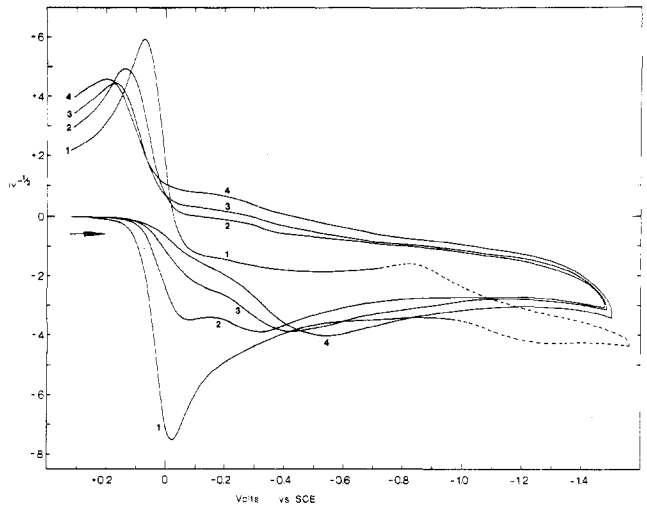

Figure 3. Normalized current ($i/v^{1/2}$) voltammograms at a stationary platinum sphere electrode for an acetonitrile solution of $[Co(mnt)_2]_2^{2-}$ (cobalt concentration 2.0×10^{-3} F) containing 1.0×10^{-2} M pyridine and 0.3 M $(Bu_4P)ClO_4$ supporting electrolyte. Voltage scan initiation is shown by the arrow. Scan rates (V/sec) are: **1**, 0.043; **2**, 0.86; **3**, 4.3; **4**, 21.5. The broke line for the trace at slowest scan rate represents spurious adsorption current.

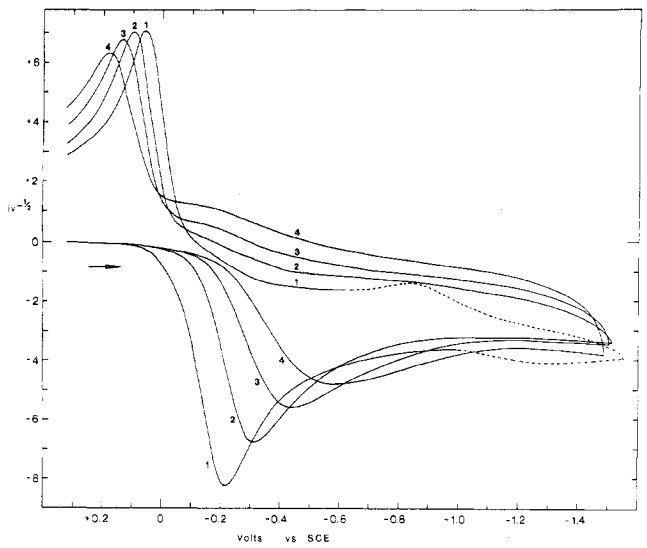

Figure 4. Normalized current ($i/v^{1/2}$) voltammograms at a stationary platinum sphere electrode for an acetonitrile solution of $[Co(mnt)_2]_2^{2-}$ (cobalt concentration 2.0×10^{-3} F) containing 1.0×10^{-1} M pyridine and 0.3 M $(Bu_4P)ClO_4$ supporting electrolyte. Voltage scan initiation is shown by the arrow. Scan rates (V/sec) are: **1**, 0.043; **2**, 0.86; **3**, 8.6; **4**, 43. The broken line for the trace at slowest scan rate represents spurious adsorption current.

equilibria. For the case (10^{-2} M pyridine, Figure 3) where the solution contains $[Co(mnt)_2]_2^{2-}$ and $[Co(mnt)_2py]^-$ in equilibrium (with the latter in excess), the reductive and oxidative peaks at the slowest scan rate (trace 1, 0.043 V sec^{-1}) are very similar to those in the absence of pyridine, except that there is a potential shift of *ca.* −70 mV. This is essentially the Nernstian shift (Appendix, section 1) of processes α/α' due to the coordinative equilibrium 1/−1. At this slow scan rate the coordinative processes 1 and −1 have negligible kinetic influence, being sufficiently fast that the pyridine adduct can dissociate (−1) or associate (1) during the period of reduction (α) or reoxidation (α'). [Notice that there is a very slight indication of current due to process β in trace 1, Figure 3, revealing that the mono-adduct dissociation (−1) is not complete during the reduc-

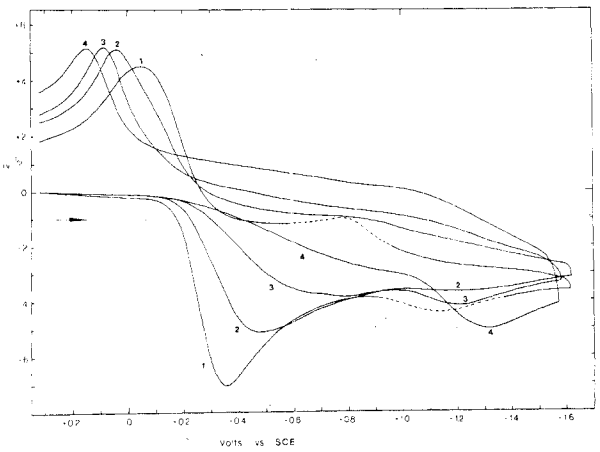

Figure 5. Normalized current ($i/v^{1/2}$) voltammograms at a stationary platinum sphere electrode for an acetonitrile solution of $[Co(mnt)_2]_2^{2-}$ (cobalt concentration 2.0×10^{-3} *F*) containing 3.0 *M* pyridine and 0.3 *M* $(Bu_4P)ClO_4$ supporting electrolyte. Voltage scan initiation is shown by the arrow. Voltage scan rates (V/sec) are: **1**, 0.043; **2**, 0.43; **3**, 4.3; **4**, 43. The broken line for the trace at slowest scan rate represents spurious adsorption current.

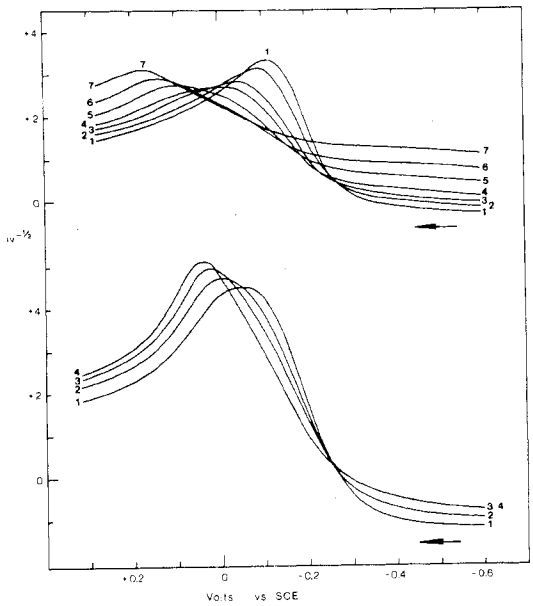

Figure 6. Normalized current ($i/v^{1/2}$) anodic voltammograms at a platinum sphere electrode of solutions of $[Co(mnt)_2]_2^{2-}$ (cobalt concentration 2.0×10^{-3} *F*) in neat pyridine (upper) and acetonitrile containing 3.0 *M* pyridine (lower). Supporting electrolyte, $(Bu_4P)ClO_4$, 0.3 *M*. Voltage scan rates (V/sec) (upper set): **1**, 0.86; **2**, 2.15; **3**, 4.3; **4**, 8.6; **5**, 21.5; **6**, 43; 7, 86; (lower set): 1, 0.043; **2**, 0.086; **3**, 0.215; 4, 0.43.

tion period at this slowest experimental scan rate.] At increasing scan rates the normalized current due to reduction α decreases while the current due to reduction β increases. This behavior is diagnostic (Appendix, section 3b, c) of a homogeneous equilibrium involving the reactants in the electron-transfer processes, in which the rate of the homogeneous process is being overtaken by the voltage scan rate. In this case the time period for reductions α and β is decreasing below the relaxation time for $[Co(mnt)_2py]^-$ dissociation, -1. The $[Co(mnt)_2]^-/[Co(mnt)_2py]^-$ equilibrium is nearly "frozen" at trace 4 (2.15 V sec^{-1}), and from the relative currents the equilibrium ratio is estimated to be *ca.* 0.1 (which is consistent with the approximate Nernstian shift mentioned above and with the spectral data).

An order of magnitude calculation of the first-order homogeneous rate constants k_1 and k_{-1} can be made by semiquantitative comparison with theory,[21-23] using the above equilibrium ratio of 0.1. The resulting values are $k_1 \simeq 1800$ sec^{-1}, $k_{-1} \simeq 180$ sec^{-1} (2.0×10^{-3} *M* $(Bu_4P)[Co(mnt)_2]$, 10^{-2} *M* pyridine). These results may be compared with those of Tsiang and Langford[24] who studied by stopped-flow methods the formation of $[Co(mnt)_2py]^-$ from $[Co(mnt)_2]_2^{2-}$ and pyridine in acetone. Reexpression of the present first-order rate constant as the specific constant k_s in the rate law

$$\frac{d[[Co(mnt)_2py]^-]}{dt} = k_s[[Co(mnt)_2]_2^{2-}]^{1/2}[py]$$

yields a value $k_s \simeq 8 \times 10^3$ $M^{-1/2}$ sec^{-1}, which agrees well with Langford's more accurate value of 8.8×10^3 $M^{-1/2}$ sec^{-1}.

The fast formation (1) of $[Co(mnt)_2py]^-$ is reflected also in the positive potential shift of the reoxidation peak (α') with increasing scan rate (Appendix, section 2c; *cf.* Figure 2). Current for the reduction α is absent in solutions with pyridine concentrations $\geq 10^{-1}$ *M*, even at the slowest scan rates employed (Appendix, section 3c).

Turning to consideration of the reduction β, there is a pronounced negative peak potential shift with increasing scan rate, clearly apparent in Figures 3-5. This is diagnostic (Appendix, section 2c) of a fast succeeding reaction, which is no doubt the dissociation ($-1'$) of $[Co(mnt)_2py]^{2-}$. However, the large magnitude of the shift, *ca.* 110 mV per log v in Figure 3, which is greater than the theoretical maximum value (30 mV per log v) plus the background value (Figure 2, *ca.* 40 mV per log v), cannot be explained. The rapid dissociation of $[Co(mnt)_2py]^{2-}$ is confirmed by the absence of its reoxidation peak β' in Figures 3 and 4 at the fastest scan rates and shortest switching times.

Comparison of the β reduction peaks in Figures 3 and 4 shows that the potential is essentially independent of pyridine concentration in the range 10^{-2}-10^{-1} *M*. This is an indication that there is no substantial change in the position of the succeeding equilibrium (Appendix, section 2d) and is therefore consistent with the description in terms of a very fast following reaction (dissociation $-1'$) independent of pyridine concentration and comparatively slow coordinative processes $1'$ and $2'$. However, in 3 *M* pyridine (Figure 5) the peak potentials for process β are found to be more negative of those for the same scan rates but lower pyridine concentrations. This negative peak potential shift could be due to the Nernstian shift of an increasingly unfavorable precursor equilibrium, 2/−2 (Appendix, section 3d).

The oxidation peak α' in Figure 4 is similar to that in Figure 3, but the potentials are slightly more negative for

(21) R. S. Nicholson and I. Shain, *Anal. Chem.*, 36, 706 (1964), case III, original notation. By comparison of current data with their Figures 3 and 4, a numerical value, x, of $\psi = (\sqrt{a}/l)(1/K)$ may be obtained for a value, y, of the scan rate (V sec^{-1}). Thence (at 25°), $k_f = 38.5yx^{-2}[K(K+1)]^{-1}$, $k_b = k_f K^{-1}$. It is to be noted that the inverse square dependence of k_b on both x and the estimated equilibrium constant ($k_{-1}/k_1 = K$) in this procedure means that errors in correlation of the observations with the theoretical curves are amplified in the derived rate constants.

(22) The correspondence between the theoretical[21] and present notation is $k_f \equiv k_{-1}$, $k_b \equiv k_1$ (all first-order rate constants). From Figure 3 (present paper) and additional unpublished data, $x = 2$ when $y = 2$ V sec^{-1} (or, equivalently, $x = 1$ when $y = 0.5$ V sec^{-1}), $k_{-1}/k_1 = 0.1$, from which $k_1 \simeq 1800$ sec^{-1}, $k_{-1} \simeq 180$ sec^{-1}.

(23) The voltammetry theory applied takes no account of the half-order dimer dissociation.

(24) H. G. Tsiang and C. H. Langford, *Can. J. Chem.*, 48, 2776 (1970).

the higher pyridine concentration at comparable scan rates. This is consistent with the Nertstian effect of the shift of equilibria 1/−1 and 2/−2 in favor of the pyridine adducts. The same direction of change is continued further in 3 *M* pyridine (Figure 5, ignoring trace 1 which conceals overlapping peaks).

The reduction γ of $[Co(mnt)_2py_2]^-$ is observed in 3 *M* pyridine at scan rates greater than 0.5 V sec^{-1} (Figure 5). This solution contains the bispyridine adduct in equilibrium with possibly a few per cent of the mono adduct. However, the rate of bis-adduct dissociation (−2) is such that at slow scan rates all of the complex can be reduced as monoadduct (β) at less negative potential. At the fastest scan rate shown (trace 4, 43 V sec^{-1}) the 2/−2 equilibrium is largely immobilized and most current flows as bis-adduct reduction γ. (It is possible that some of the current function decrease for reduction β in Figure 4 at the higher scan rates may reflect limited −2 relaxation.) A very approximate calculation based on the traces in Figure 5, assuming the equilibrium ratio $[Co(mnt)_2py]^-/[Co(mnt)_2py_2]^-$ to be 0.05, and estimating that the kinetic current in β is halved at a scan rate of 2 V sec^{-1}, yields[21] first-order rate constants of 2×10^3 sec^{-1} for dissociation 2′ and 4×10^4 sec^{-1} for association 2. In conventional notation

$$K_2 = \frac{[[Co(mnt)_2py_2]^-]}{[[Co(mnt)_2py]^-][py]} = \frac{k_2^{(2)}}{k_{-2}^{(1)}} = \frac{1.3 \times 10^4\ M^{-1}\ sec^{-1}}{2 \times 10^3\ sec^{-1}} = 7\ M^{-1}$$

There is a pronounced negative shift of the γ peak potential with increasing scan rate, reflecting the very fast dissociation (−2′) of the product $[Co(mnt)_2py_2]^{2-}$. From a comparison of Figures 4 and 5 it can be concluded that the dissociation dynamics for $[Co(mnt)_2py_2]^{2-}$ in 3 *M* pyridine are similar to those of $[Co(mnt)_2py]^{2-}$ in 0.1 *M* pyridine.

Oxidation of $[Co(mnt)_2py]^{2-}$. In neat pyridine (Figure 6) two separate oxidations occur with $E_p = -0.11$ V and $E_p \sim +0.15$ V and are assigned as β' and α', respectively. There is no current due to oxidation α' at scan rates less than about 1 V sec^{-1} and barely detectable current due to oxidation β' at the fastest scan rate, 86 V sec^{-1} (trace 7, Figure 6). This reflects the mobility of the equilibrium 1′/−1. The β' current increases (and α' current decreases) with pyridine concentration from 3 to 12.4 *M* at constant scan rate. All of these observations indicate that at high pyridine concentrations the rate of association $[Co(mnt)_2]^{2-} + py \rightarrow [Co(mnt)_2py]^{2-}$ is sufficiently fast that at the slower scan rates appreciable kinetic current flows in oxidation of $[Co(mnt)_2py]^{2-}$. The equilibrium concentration ratio, $K = [[Co(mnt)_2py]^{2-}]/[[Co(mnt)_2]^{2-}]$, is unknown but probably not greater than 0.05. By comparison with theory[21] the first-order rate constant for monopyridine adduct formation (1′) is estimated to be $10[K(K+1)]^{-1}$ sec^{-1} (from which, with [py] = 12.4 *M*, and a value of *K*, other rate constants may be calculated). The adduct $[Co(mnt)_2py]^{2-}$ has not yet been identified by other techniques under equilibrium conditions[25] (the voltammetric manifestation being a nonequilibrium phenomenon).

In neat pyridine solution at slow scan rates (<1 V sec^{-1}) a single voltammetric "duck" is observed, with normal reversible appearance and $i_p^c = i_p^a$. The peak and midpoint potentials are illustrated in Table I. The peaks are the reduction and oxidation of $[Co(mnt)_2py]^-$, β and β', but *both* represent almost totally *kinetic* currents, as $[Co(mnt)_2py_2]^-$ and $[Co(mnt)_2]^{2-}$ are the equilibrium species in oxidized and reduced solutions, respectively. The tabulated midpoint potential then represents the β/β' redox potential, as influenced by Nernstian displacements, to more negative potentials by the 2/−2 equilibrium and to more positive potentials by the 1′/−1′ equilibrium. Magnitudes of the Nernstian shifts cannot be evaluated with the data available. However, all observations are consistent with the equilibrium condition $k_{-1'}/k_{1'} \gg k_2/k_{-2}$, even at high concentrations, which leads to the prediction that the β/β' thermodynamic potential is considerably more negative than −0.3 V. This conclusion is supported by the pronounced negative shift of the β peak potential with increasing scan rate in Figures 3–5 (Appendix, section 3d).

Table I. Peak Potentials for $(Bu_4P)[Co(mnt)_2]$ in Neat Pyridine[a]

Scan rate v, V/sec	E_p^c	E_p^a	$\frac{1}{2}\Sigma E_p$
0.0215	−0.330	−0.185	−0.26
0.043	−0.355	−0.175	−0.27
0.086	−0.380	−0.160	−0.27
0.215	−0.46	−0.14	−0.30

[a] Potentials in volts *vs.* sce. $(Bu_4P)[Co(mnt)_2]$, 2×10^{-3} *M*; Bu_4PClO_4, 0.3 *M*.

By way of conclusion it can be reaffirmed that all of the voltammetric observations on the $[Co(mnt)_2]^{1-/2-}$-pyridine system are consistent with the array of processes shown in Scheme II. The simple utility of the voltammetric method for semiquantitative estimation of the homogeneous equilibrium and rate constants has been illustrated. However, it must also be stated that this method depends upon the achievement of appropriate solution conditions, such as homogeneous relaxation times which are within the voltammetric time scale. Also it is unlikely that very much higher accuracy will be attained in nonaqueous systems such as these, due to uncertainties in the experiments and the model.

Summary

1. The utility of stationary electrode voltammetry in semiquantitative characterization of the dynamics of coordinative reactions for electron-transfer active complexes has been demonstrated.

2. The reduction of $[Co(mnt)_2]_2^{2-}$, $[Co(mnt)_2py]^-$, and $[Co(mnt)_2py_2]^-$ and the oxidation of $[Co(mnt)_2]^{2-}$ and $[Co(mnt)_2py]^{2-}$ were observed under various conditions, but there was no evidence for oxidation of $[Co(mnt)_2py_2]^{2-}$.

3. The equilibrium and rate constants for $\frac{1}{2}[Co(mnt)_2]_2^{2-} + py \rightleftarrows [Co(mnt)_2py]^-$ were estimated and found to be in good agreement with data from other sources.

4. The equilibrium and rate constants for $[Co(mnt)_2py]^- + py \rightleftarrows [Co(mnt)_2py_2]^-$ were estimated.

$$K_2 = \frac{[[Co(mnt)_2py_2]^-]}{[[Co(mnt)_2py]^-][py]} = \frac{k_2^{(2)}}{k_{-2}^{(1)}} = \frac{1.3 \times 10^4\ M^{-1}\ sec^{-1}}{2 \times 10^3\ sec^{-1}} = 7\ M^{-1}$$

5. The reduced adduct, $[Co(mnt)_2py]^{2-}$, was detected by its oxidation under nonequilibrium conditions, and the equilibrium

$$[Co(mnt)_2]^{2-} + py \rightleftarrows [Co(mnt)_2py]^{2-}$$

was partially characterized.

$$K_{1'} = \frac{[[Co(mnt)_2py]^{2-}]}{[[Co(mnt)_2]^{2-}][py]} < 4 \times 10^{-3}\ M^{-1}$$

(25) The existence of low concentrations of $[Co(mnt)_2PEt_3]^{2-}$ in solution when PEt_3 is added to $[Co(mnt)_2]^{2-}$ has been suggested[4] on the basis of the ease of oxidation by oxygen.

$$\frac{\frac{d}{dt}[Co(mnt)_2py]^{2-}}{[[Co(mnt)_2]^{2-}][py]} = k_1'^{(2)} \simeq$$
$$0.8[12.4K_1'(12.4K_1' + 1)]^{-1}\ M^{-1}\ sec^{-1}$$

Acknowledgments. This research was supported by the National Science Foundation (GP 24443X). Enlightening discussions with Professor D. H. Evans are acknowledged.

Appendix

The theory of electrochemistry is independent of the direction of electron transfer, and therefore it becomes convenient to express the phenomenology of stationary electrode voltammetry in generalized form applicable to both oxidation and reduction experiments. This removes the normal definition of sign for the potential axis, but it is readily replaced by a sufficient and general definition based only on the product (and by implication the reactant) of the electron-transfer process. Thus, the direction of potential change which would produce, by electron transfer, species B from species A (as defined in the chemical model) is denoted potential direction B, while the opposite direction is termed A. Then, if the electron-transfer process A → B is under discussion, the potential direction B may be described as "with" the direction of electron transfer and potential direction A as "against" the direction of electron transfer. It is also convenient to characterize observed voltammetric *peak potential shifts*, induced by change in an independent experimental variable, as "with" (parallel to) or "against" (antiparallel to) the direction of electron transfer which is responsible for the voltammetric peak.[26,27] The theory summarized in the following statements assumes that heterogeneous electron transfer with the electrode is not rate limiting (*i.e.*, *electrochemical* reversibility is maintained) and that homogeneous processes exert the thermodynamic or kinetic control.

1. Effects When All Homogeneous Processes Maintain Equilibrium.[28] The electron-transfer potential (E_p or $E_{1/2}$) reflects the homogeneous equilibria in the well-known Nernstian manner. The general statement of direction for the Nernstian potential shift is that upon displacement of any homogeneous equilibrium the electron-transfer potential is shifted away from an electroactive species whose concentration is decreased and toward an electroactive species whose concentration is increased.

2. Kinetic Control in a Homogeneous Equilibrium Involving the Product of Electron-Transfer Reaction.[29,30] The system may be described by the equation

$$B^{\pm} \rightarrow B \underset{k_A}{\overset{k_B}{\rightleftharpoons}} A$$

(a) Changes in the normalized current function over the full range of kinetic variables are less than 10%. Current function constancy has confirmatory but not diagnostic value.

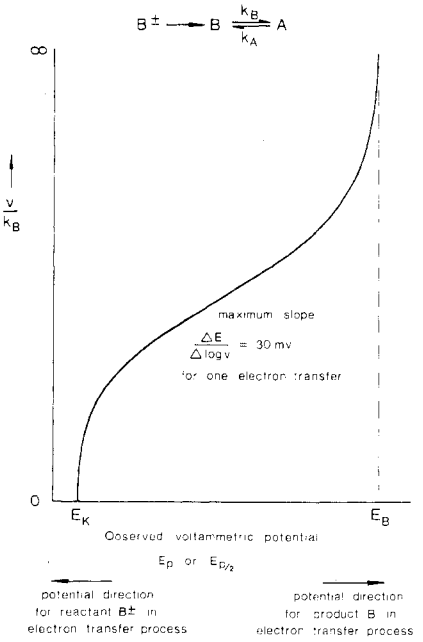

Figure 7. Dependence of observed voltammetric potential upon the potential scan rate, v, when the product of electron transfer is involved in a homogeneous process.

(b) Peak potential shifts are the primary indicator of the homogeneous processes. Substantial shifts may occur, as represented in Figure 7. As one limiting case, when $v \ll\ll k_B$, the homogeneous equilibrium is maintained, and the Nernstian potential, E_K, is observed (the equilibrium constant being k_B/k_A). At the other limit, when $v \gg\gg k_B$, the homogeneous reaction B → A cannot occur during the voltammetric experiment, and the normal $B^{\pm}/B$ potential, E_B, is observed. Between these limits the observed voltammetric potential shows sigmoid variation with v/k_B (see Figure 7). If v is the independent experimental variable, the maximum slope $\Delta E/\Delta \log v$ is 30 mV[31] for one electron transfer. The range of scan rates v over which this maximum $\Delta E/\Delta \log v$ obtains is dependent on k_A as well as k_B.

(c) The qualitatively useful, generalized diagnostic for a kinetically controlling homogeneous reaction of the electron-transfer product is that for experiments with increasing v the voltammetric potential will shift in the direction of the electron-transfer product; the rate of shift, $\Delta E/\Delta \log v$, will increase to its maximum value as the scan rate approaches $0.01 \times (k_A/k_B)^2(k_A + k_B)$;[31,32] at considerably higher scan rates the potential will asymptotically approach E_B. It is to be noted that the variation in v necessary to reveal the full sigmoid variation of E covers many decades, which will not in general be experimentally accessible.

(d) The effect of equilibrium constant change (*via* k_B and/or k_A) at constant scan rate is to shift the potential in Nernstian sense.

3. Kinetic Control in a Homogeneous Equilibrium Involving the Reactant in the Electron-Transfer Reaction.[33] The system is

$$A \underset{k_B}{\overset{k_A}{\rightleftharpoons}} B \rightarrow B^{\pm}$$

(26) For example, a shift of a reduction voltammetric peak to more negative potentials is "with" electron transfer, while a negative shift of an oxidative voltammetric peak is "against" the direction of electron transfer.

(27) The effect of increasing electrochemical irreversibility, or of increasing uncompensated cell resistance, is to shift the observed peak potential in the direction of electron transfer.

(28) Homogeneous equilibrium is maintained when the half-lives of all homogeneous transformations are much less than the minimum period during which the potential of the working electrode is changed by 50 mV.

(29) The unidirectional voltammetric experiment is implied in this discussion, not the cyclic voltammetric experiment for which the theory of sections 2 *and* 3 must be combined.

(30) The quantitative theory is given as cases V and VI, single scan method, of ref 13.

(31) The units for the scan rate are volts per time unit of the first-order rate constants k_A and k_B.

(32) This *approximate* calculation is based on Figure 9 of ref 13, which should be used for quantitative work.

(33) The quantitative details are given as case III in ref 13.

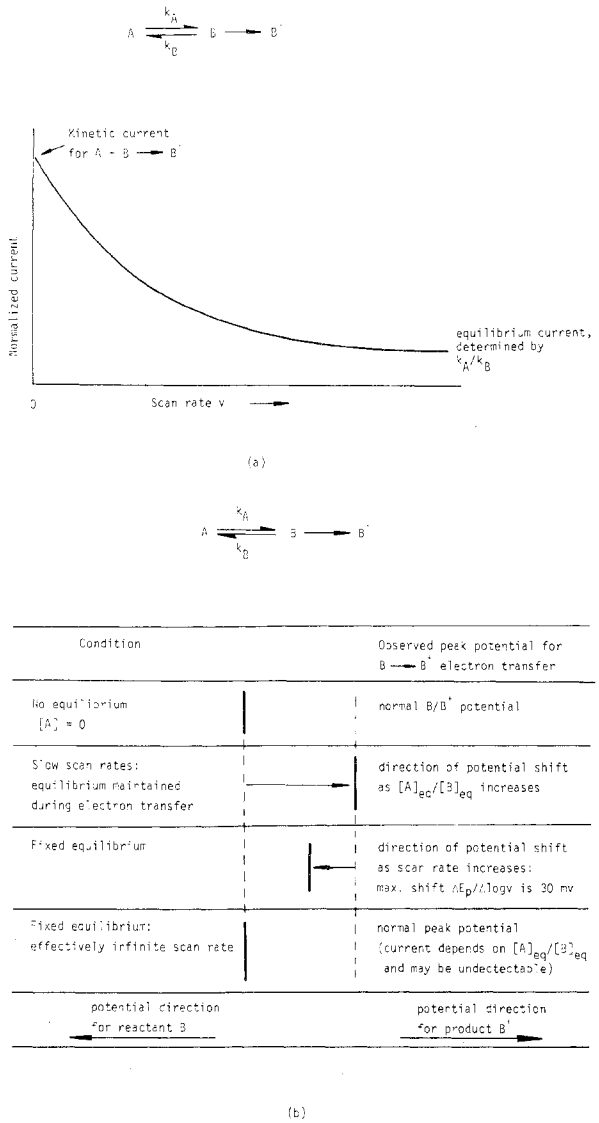

Figure 8. Qualitative representation of voltammetric normalized peak current (a) and peak potential (b) dependence on potential scan rate and homogeneous equilibrium position for the case where the reactant in the heterogeneous electron-transfer process is involved in a homogeneous equilibrium.

(a) In contrast to 2, the kinetic influence of k_A and k_B is manifested primarily in the current function.

(b) This case becomes distinguishable to the extent that the equilibrium is away from the electron-transfer reactant (*i.e.*, when $[A]_{eq}/[B]_{eq}$ is appreciable). The observed current depends on the ratio of the homogeneous equilibrium relaxation time to the period for electron transfer, that is, the time to scan *ca.* 100 mV. In the limit of scan rates very much faster than the homogeneous chemical rates the equilibrium is effectively frozen, and the current function is proportional to the equilibrium concentration of the electroactive species B. On the other hand, at very slow relative scan rate the homogeneous equilibria can be maintained (by $A \rightarrow B$) during the period of electron transfer ($B \rightarrow B^{\pm}$) and enhanced kinetic currents are observed corresponding to conversion of all A and B to $B^{\pm}$.

(c) Kinetic currents decrease to equilibrium currents as the scan rate increases, as shown in Figure 8a.[33,34] When the chemical equilibrium is displaced strongly away from the electroactive species, $[A]_{eq}/[B]_{eq} = k_B/k_A \gg 1$, even the slowest scan rate cannot induce relaxation of the equilibrium, and no current is observed (electron transfer is unable to compete with k_B for B).

(d) Peak potential shifts are dependent on both the scan rate and the homogeneous equilibrium constant. The behavior is summarized qualitatively in Figure 8b.

At sufficiently slow relative scan rate the observed potential of the kinetic current peak is dependent on the homogeneous equilibrium constant in Nernstian sense. As the scan rate increases and the equilibrium becomes immobilized, the observed potential shifts toward E_B which is in the direction of the electron-transfer reactant B. However, the peak also becomes drawn out with this change and may effectively disappear if $[B]_{eq} \ll [A]_{eq}$.

Registry No. $(Bu_4P)_2[Co(mnt)_2]$, 40895-20-3; $(Bu_4P)_2[Co(mnt)_2]_2$, 41004-09-5; $(Bu_4P)_2[Ni(mnt)_2]$, 40895-21-4; $(Bu_4P)[Ni(mnt)_2]$, 40959-48-6; py, 110-86-1; $[Co(mnt)_2py]^-$, 41004-10-8; $[Co(mnt)_2py_2]^-$, 40895-22-5; $[Co(mnt)_2py]^{2-}$, 40959-49-7.

(34) Homogeneous rate constants may be evaluated[21] from experimental data lying on the steep part of the curve in Figure 8a. The accessibility of this data region is increased when it is possible to vary the rates $A \rightarrow B$ and $B \rightarrow A$ independently (*via* ligand concentrations, for instance).